Supplement

Signature of the stratosphere-troposphere coupling on recent record-breaking Antarctic sea ice anomalies

Raúl R. Cordero[1,2], Sarah Feron[2]*, Alessandro Damiani[3], Pedro J. Llanillo[4], Jorge Carrasco[5], Alia L. Khan[6,7], Richard Bintanja[8,9], Zutao Ouyang[10], Gino Casassa[5]

[1]Universidad de Santiago de Chile. Av. Bernardo O'Higgins 3363, Santiago, Chile.
[2]University of Groningen, Wirdumerdijk 34, 8911 CE, Leeuwarden, The Netherlands.
[3]Center for Environmental Remote Sensing, Chiba University, 1-33 Yayoicho, Inage Ward, Chiba, 263-8522, Japan.
[4]Alfred-Wegener-Institute Helmholtz Center for Polar and Marine Research, Am Handelshafen 12, 27570 Bremerhaven, Germany
5University of Magallanes, Av. Manuel Bulnes 1855, 621-0427 Punta Arenas, Chile
[6]Western Washington University, 516 High St, Bellingham, WA 98225, USA.
[7]National Snow and Ice Data Center, Cooperative Institute for Research in Environmental Sciences, University of Colorado—Boulder, 449 UCB University of Colorado Boulder, CO 80309-0449 USA.
[8]Royal Netherlands Meteorological Institute (KNMI), Utrechtseweg 297, 3731 GA De Bilt, The Netherlands.
[9]Energy and Sustainability Research Institute Groningen (ESRIG), University of Groningen, Groningen, The Netherlands.
[10]Department of Earth System Science, Stanford University, 473 Via Ortega, Stanford, CA, 94305-2210, USA.

Correspondence to: Sarah Feron (s.c.feron@rug.nl)
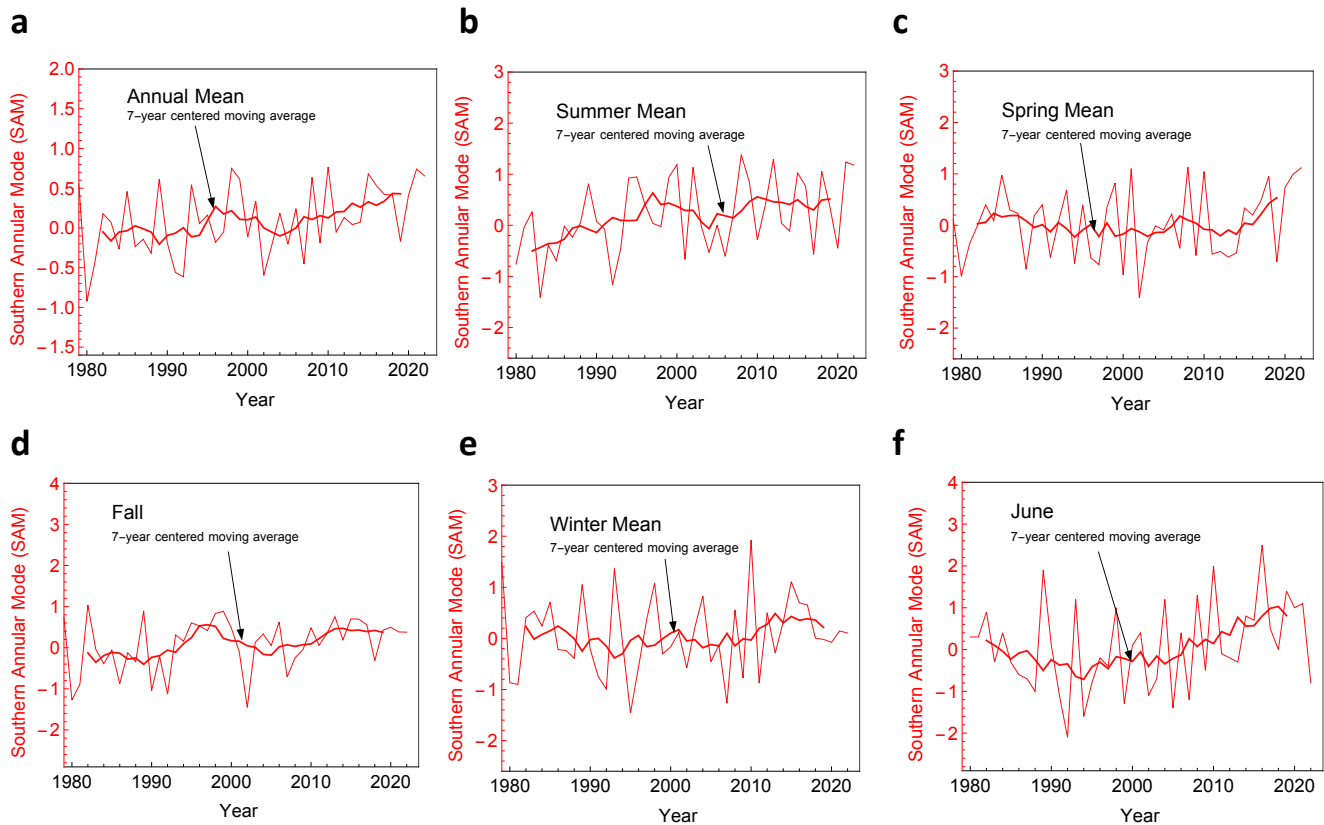
Figure S1

(a) Annual mean of the Southern Annular Mode (SAM) index. There is a long-term trend toward positive values of the SAM index. In 2022, the annual mean of the SAM index ended in positive values for the third year in a row.

(b) Mean SAM index for summer (DJF). Attributable to the success of the Montreal Protocol, there has been a pause in the long-term strengthening of the summertime SAM.

(c) Mean SAM index for spring (SON). The highest spring SAM average since 2008 occurred in 2022.

(d) Mean SAM index for fall (MAM).

(e) Mean SAM index for winter (JJA).

(f) Mean SAM index for early winter (June). In 2022 occurred the lowest SAM average for June since 2007.

The bold red line shows the 7-year centered moving average. Estimates of the SAM index were obtained from Climate Prediction Center (National Weather Service, National Oceanic and Atmospheric Administration – NOAA (Mo, 2000)). Plots were generated using Python's Matplotlib library (Hunter, 2017).
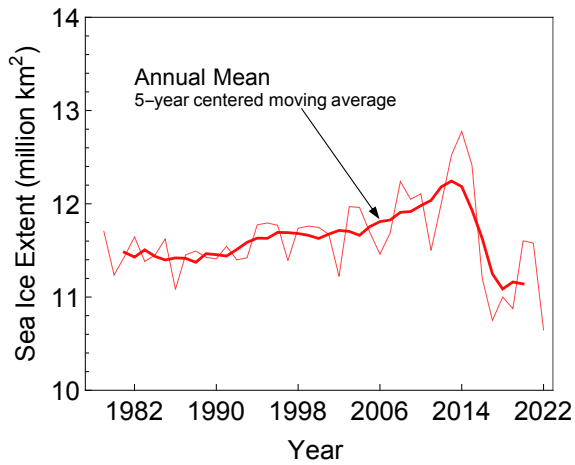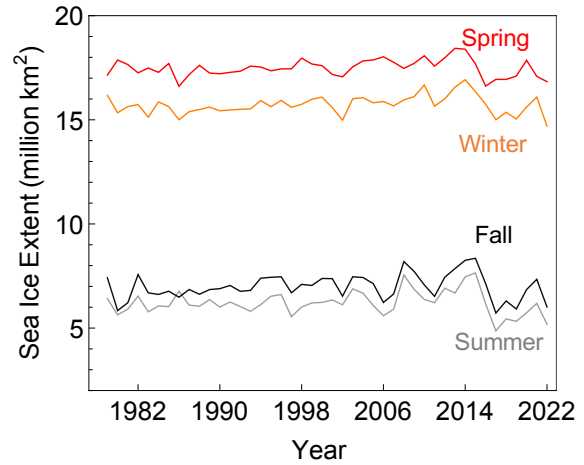
Figure S2

(a) Annual mean of the sea ice extent around Antarctica. In 2022, the sea ice extent reached its lowest annual mean since the start of satellite observations, surpassing the previous record of 2017.

(b) Mean Sea ice extent for each season.

Sea ice data were obtained from the U.S. National Snow and Ice Data Center Sea Ice Index (Fetterer et al., 2017). Plots were generated using Python's Matplotlib library (Hunter, 2017).
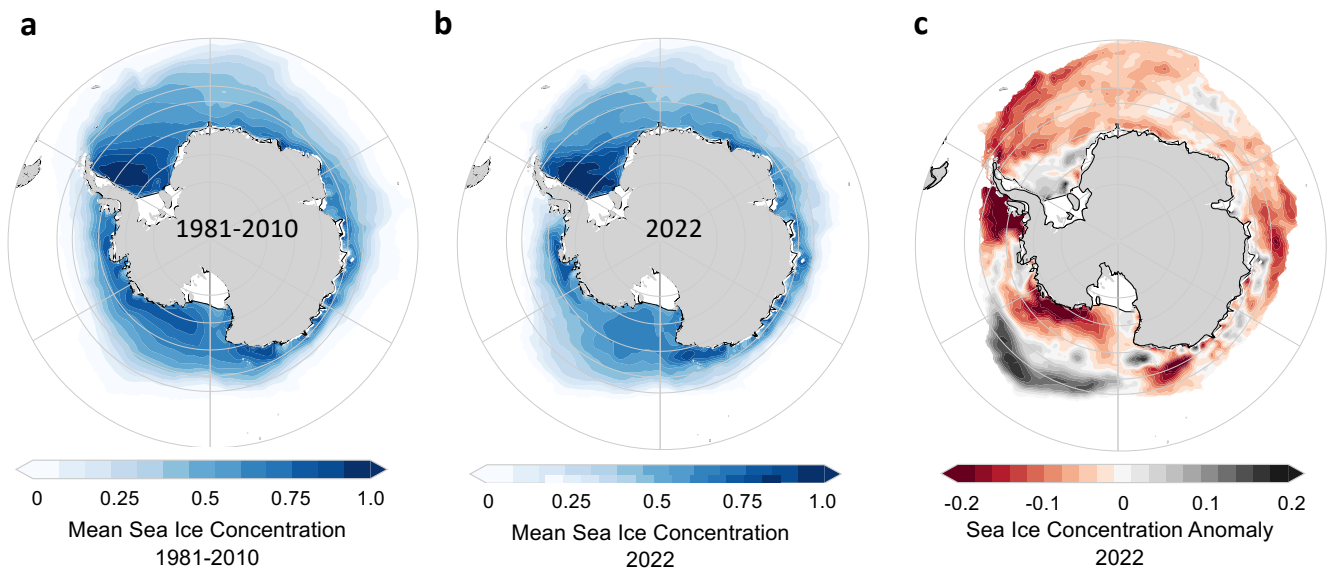
Figure S3

(a) Sea ice concentration averaged over the period 1981–2010.

(b) Sea ice concentration averaged for 2022.

(c) Sea ice concentration anomalies relative to 1981-2010 mean. Negative (positive) anomalies are apparent in the Bellingshausen (Ross) Sea sector.

Sea ice data were obtained from the U.S. National Snow and Ice Data Center Sea Ice Index (Fetterer et al., 2017). Plots were generated using Python's Matplotlib library (Hunter, 2017).

a 2022

b 2017

Sea Level Pressure Anomaly (hPa)

-8   -4   0   +4   +8
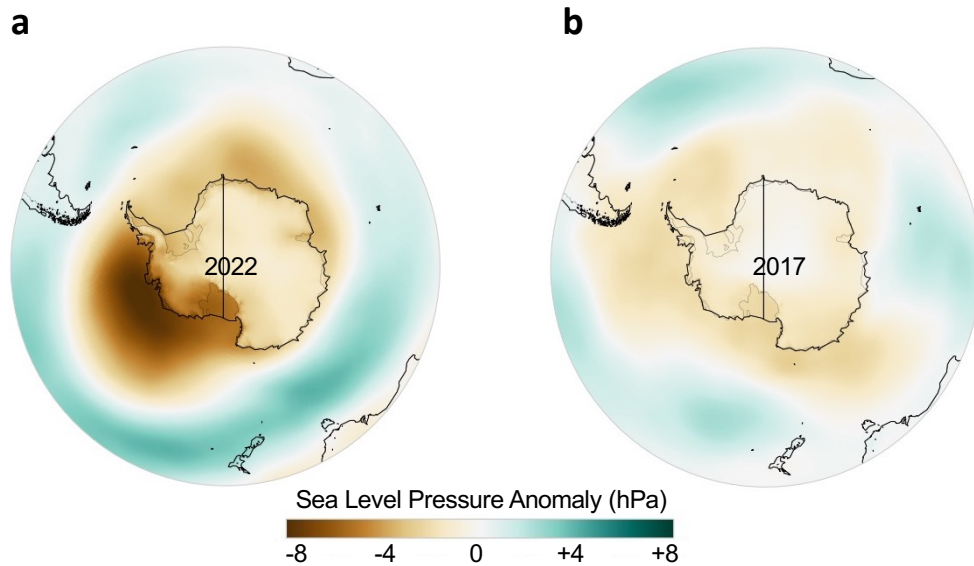
Figure S4

Annual sea-level pressure anomalies relative to the 1981-2010 mean. The Amundsen Sea Low has deepened since the mid-20th century. While Amundsen Sea Low reached record low levels in 2022 (**a**), it was close to the long-term average in 2017 (**b**). Despite the sharp differences in the deep of the Amundsen Sea Low, the sea ice extent around Antarctica dropped to comparable record lows in 2022 and in 2017.

Data comes from the ECMWF atmospheric reanalysis ERA5 (Hersbach, 2016). Plots were generated using Python's Matplotlib library (Hunter, 2017).
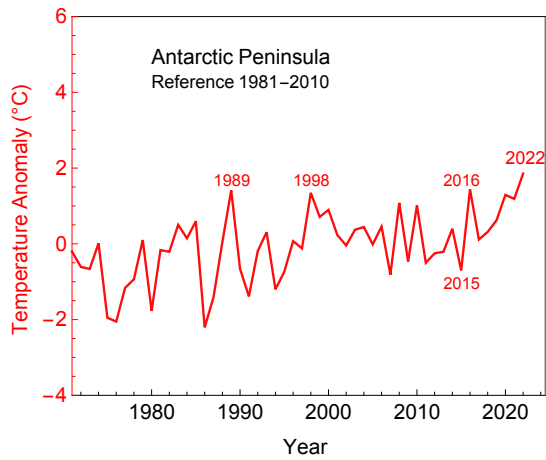
a   **b**
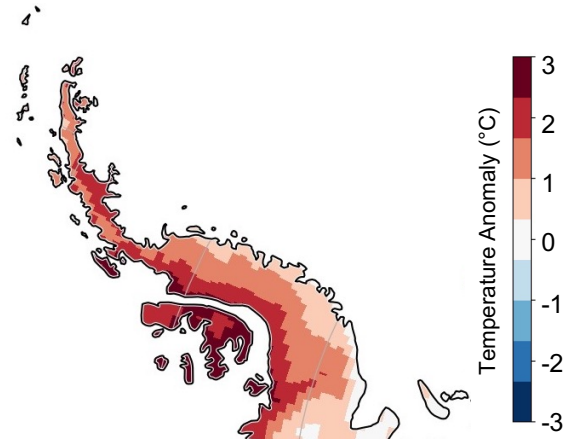
Figure S5

Annual temperature anomalies in the Antarctic Peninsula relative to the 1981-2010 mean.

(a) Time series of the annual mean temperature. The Antarctic Peninsula had in 2022 its warmest year on record.

(b) Regional pattern of the annual temperature anomalies for 2022.

Data comes from the ECMWF atmospheric reanalysis ERA5 (Hersbach, 2016). Plots were generated using Python's Matplotlib library (Hunter, 2017).

Figure S6
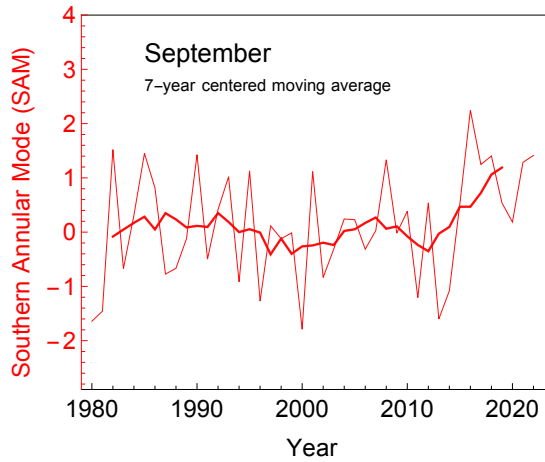
(a) Mean SAM index for September. The bold red line shows the 7-year centered moving average.

(b) Top 10 highest mean SAM values for September. Five of the ten largest positive SAM anomalies occurred since 2016.

Estimates of the SAM index were obtained from Climate Prediction Center (National Weather Service, National Oceanic and Atmospheric Administration – NOAA (Mo, 2000)). Plots were generated using Python's Matplotlib library (Hunter, 2017).
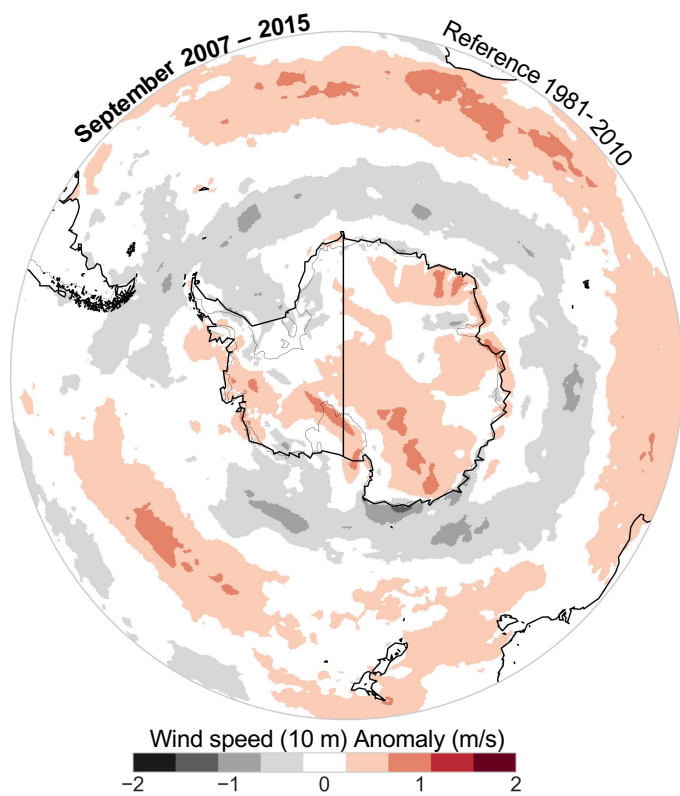
Figure S7

Average near-surface wind speed for September 2007-2015 relative to the 1981–2010 mean. Over the period 2007-2015, westerly winds around Antarctica were in early spring (September) slightly below the 1981–2010 climatology.

Data of the near-surface wind speed comes from the ECMWF atmospheric reanalysis ERA5 (Hersbach, 2016). Plot was generated using Python's Matplotlib library (Hunter, 2017).
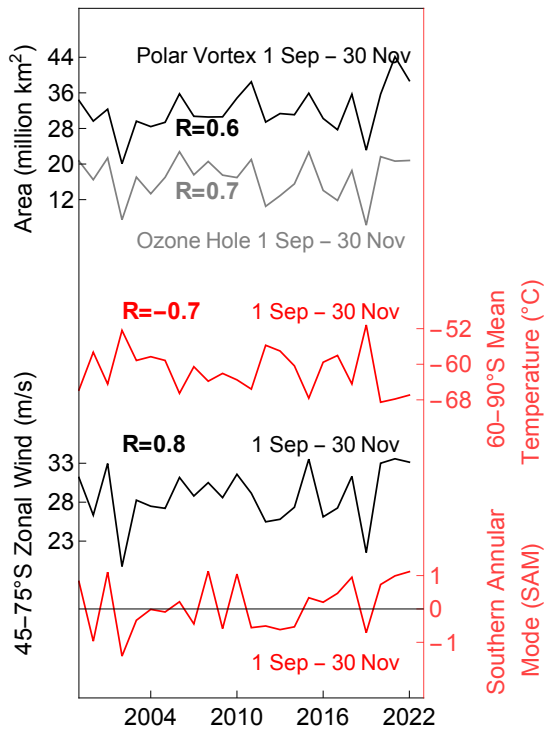
Figure S8

Spring averages of the SAM index (red line, lower panel), the 45-75° zonal mean zonal wind speed on the 100-hPa surface (black line, middle panel), the 60-90° zonal mean zonal temperature on the 50-hPa surface (red line, middle panel), the ozone hole area (gray line, upper panel), and the polar vortex area on the 460-K isentropic surface (black line, upper panel). In every case, daily estimates were averaged from 1 September to 30 November. The correlation coefficients (R) between the SAM index and the stratospheric temperature, the stratospheric wind speed, the ozone hole area, and the polar vortex area are shown in the plot.

Daily estimates of the SAM index were obtained from Climate Prediction Center (National Weather Service, National Oceanic and Atmospheric Administration – NOAA (Mo, 2000)). Daily estimates of the 45-75° zonal mean zonal wind speed, the 60-90° zonal mean zonal temperature, the ozone hole area, and the polar vortex area on the 460-K isentropic surface are from the Modern-Era Retrospective analysis for Research and Applications, Version 2 (MERRA-2) assimilation (Gelaro et al., 2017). Plots were generated using Python's Matplotlib library (Hunter, 2017).
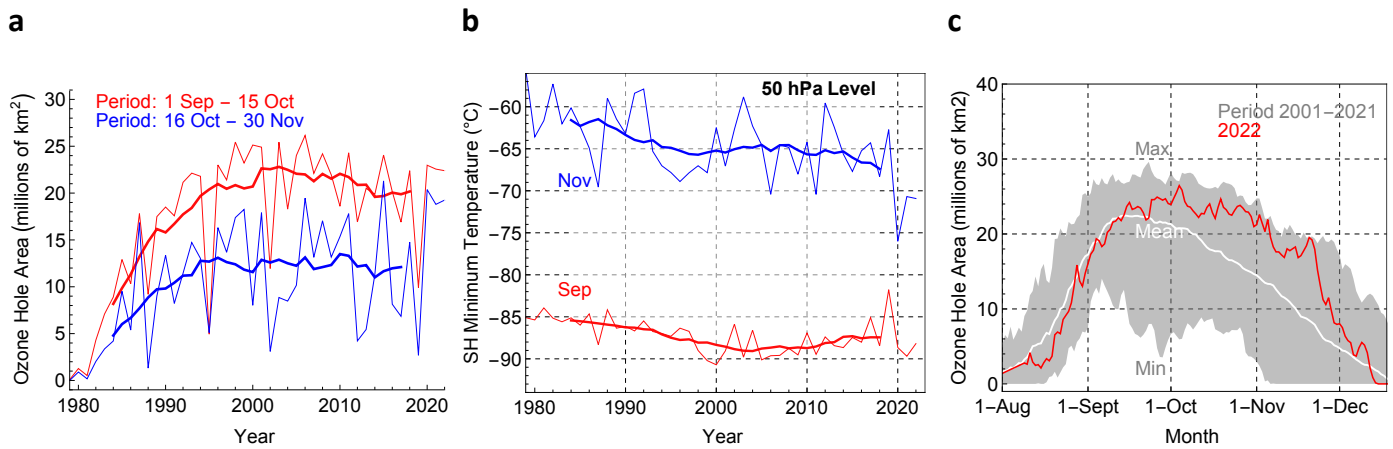
Figure S9

(a) Progress of ozone hole area averaged from 1 September to 15 October (red line) and from 16 October to 30 November (blue line). Bold lines show 11-year centered moving averages.

(b) Mean Southern Hemisphere (SH) minimum temperature for November (blue) and for September (red) at the 50 hPa Level. Bold lines show 11-year centered moving averages.

(c) Progress of the total ozone column for 2022 (red line). The gray shading indicates the highest and lowest values measured over the period 2001–2021 while the white line indicates the mean over the same period.

Estimates of the ozone hole area, and the SH minimum temperature are from the Modern-Era Retrospective analysis for Research and Applications, Version 2 (MERRA-2) assimilation (Gelaro et al., 2017). Plots were generated using Python's Matplotlib library (Hunter, 2017).

a

September
7–year centered moving average

b

Year	Top 15 highest 45-75° zonal mean zonal wind speeds for September (m/s)
2021	36.7
1982	36.4
2015	35.9
2001	35.8
1992	35.6
1998	35.6
2022	35.4
1995	35.2
1993	35.2
1987	34.9
1990	34.9
2018	34.7
2020	34.7
2016	34.4
1985	34.3
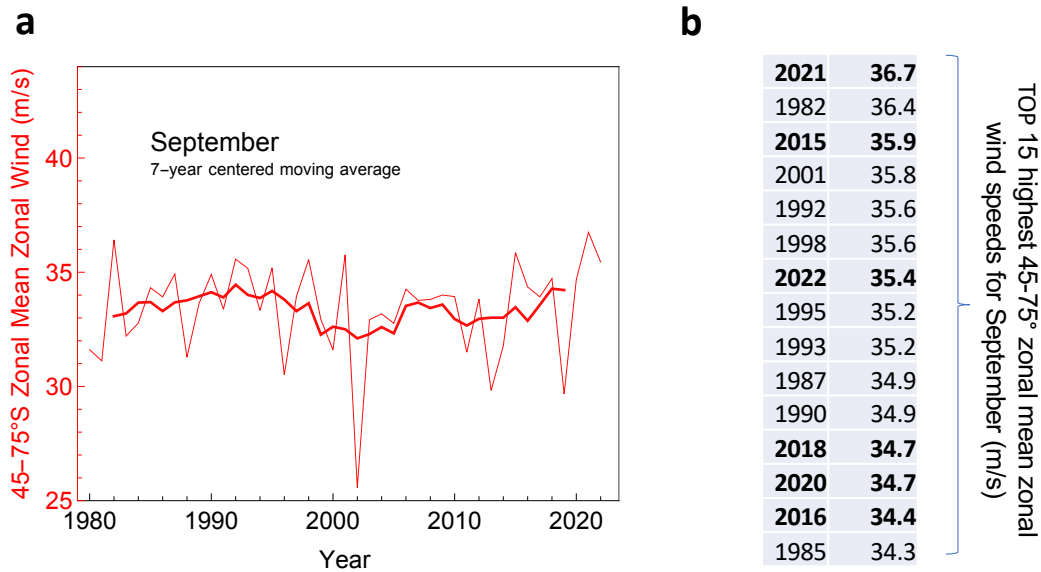
Figure S10

(a) 45-75° zonal mean zonal wind speed on the 100-hPa surface for September. The average east-west (zonal) wind speed for 45°S to 75°S is near the peak of the polar jet maximum. The bold red line shows the 7-year centered moving average.

(b) Top 15 highest 45-75° zonal mean zonal wind speed on the 100-hPa surface for September. Six of the TOP 15 highest mean 45-75° zonal mean zonal wind speeds for September occurred during the last decade.

Estimates of the 45-75° zonal mean zonal wind speed are from the Modern-Era Retrospective analysis for Research and Applications, Version 2 (MERRA-2) assimilation (Gelaro et al., 2017). Plots were generated using Python's Matplotlib library (Hunter, 2017).
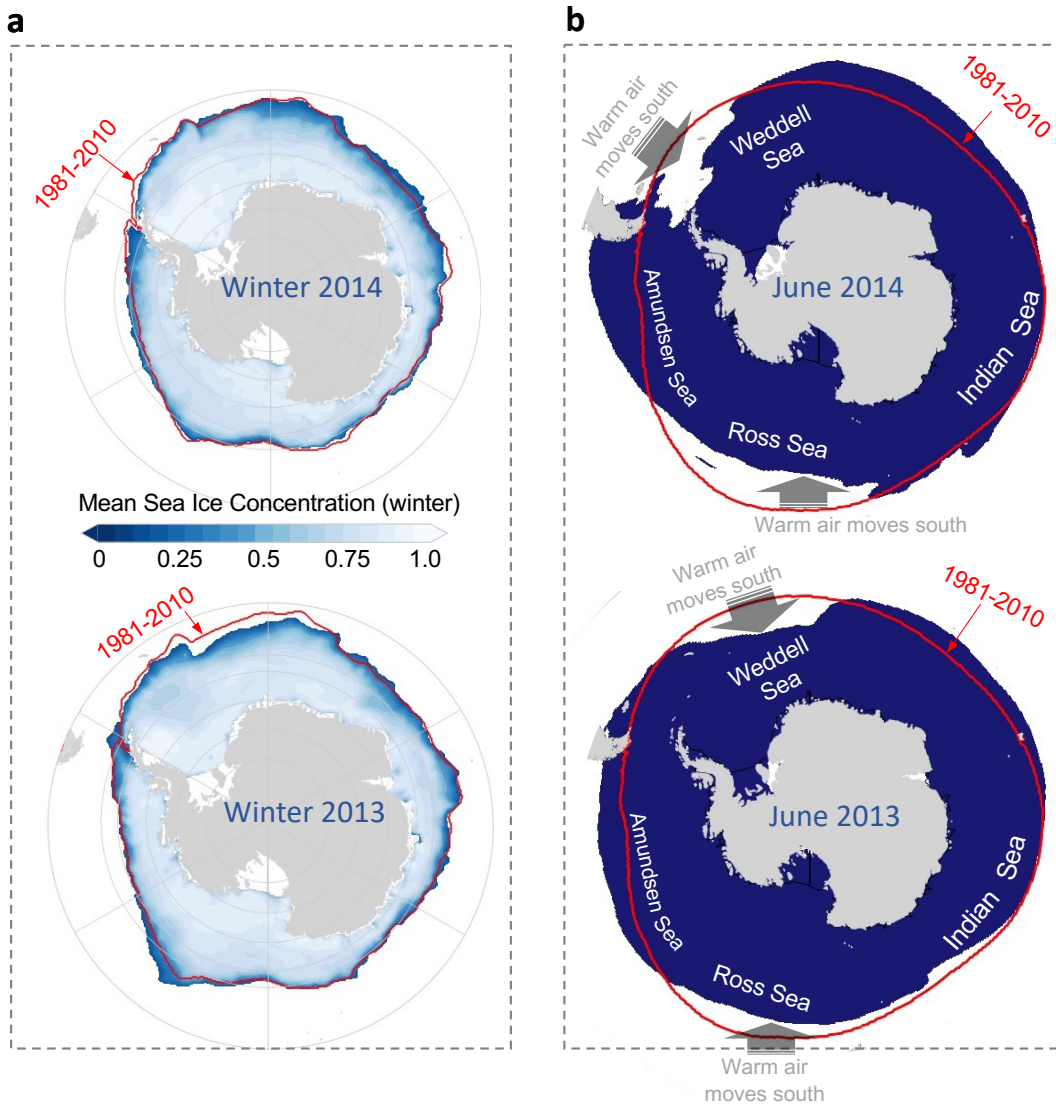
Figure S11.

(**a**) Sea ice concentration for winter 2014 (upper panel) and for winter 2013 (lower panel). The spring ice edge averaged over the period 1981–2010 is also shown (red line). The ice edge was defined applying a 0.15 threshold. Relative to 1981-2010 climatology, there are several anomalies apparent. Slightly negative anomalies in the western Weddell Sea sector in winter 2014 as well as negative anomalies in the Weddell Sea sector in winter 2013.

(**b**) Polar vortex (100 hPa) for June 2014 (upper panel) and for June 2013 (lower panel). The June vortex edge averaged over the period 1981–2010 is also shown (red line). The vortex edge was defined applying a 1.2×10^{-5} K kg^{-1} m^2 s^{-1} threshold to the potential vorticity on the 100 hPa pressure surface. Relative to 1981-2010 climatology, there are several anomalies apparent. Negative anomalies in the western Weddell Sea sector in winter 2014 as well as in the Weddell Sea sector in winter 2013.

Sea ice data were obtained from the U.S. National Snow and Ice Data Center Sea Ice Index (Fetterer et al., 2017). The potential vorticity data comes from the ECMWF atmospheric reanalysis ERA5 (Hersbach, 2016). Plots were generated using Python's Matplotlib library (Hunter, 2017).